4-2016

Optogenetic Control of Calcium Oscillation Waveform Defines NFAT as an Integrator of Calcium Load

Pimkhuan Hannanta-anan
University of Pennsylvania, pimh@seas.upenn.edu

Brian Y. Chow
University of Pennsylvania, bchow@seas.upenn.edu

Optogenetic Control of Calcium Oscillation Waveform Defines NFAT as an Integrator of Calcium Load

Abstract
It is known that the calcium-dependent transcription factor NFAT initiates transcription in response to pulsatile loads of calcium signal. However, the relative contributions of calcium oscillation frequency, amplitude, and duty cycle to transcriptional activity remain unclear. Here, we engineer HeLa cells to permit optogenetic control of intracellular calcium concentration using programmable LED arrays. This approach allows us to generate calcium oscillations of constant peak amplitude, in which frequency is varied while holding duty cycle constant, or vice versa. Using this setup and mathematical modeling, we show that NFAT transcriptional activity depends more on duty cycle, defined as the proportion of the integrated calcium concentration over the oscillation period, than on frequency alone. This demonstrates that NFAT acts primarily as a signal integrator of cumulative load rather than a frequency-selective decoder. This approach resolves a fundamental question in calcium encoding and demonstrates the value of optogenetics for isolating individual dynamical components of larger signaling behaviors.

Disciplines
Biomedical Engineering and Bioengineering | Engineering

Optogenetic control of calcium oscillation waveform defines NFAT as an integrator of calcium load

Pimkhuan Hannanta-anan and Brian Y. Chow (*)

Department of Bioengineering, University of Pennsylvania, Philadelphia, PA 19104, USA.

(*) Correspondence: bchow@seas.upenn.edu

Summary: It is known that the calcium-dependent transcription factor NFAT initiates transcription in response to pulsatile loads of calcium signal. However, the relative contributions of calcium oscillation frequency, amplitude, and duty cycle to transcriptional activity remain unclear. Here, we engineer HeLa cells to permit optogenetic control of intracellular calcium concentration using programmable LED arrays. This approach allows us to generate calcium oscillations of constant peak amplitude, in which frequency is varied while holding duty cycle constant, or vice versa. Using this setup and mathematical modeling, we show that NFAT transcriptional activity depends more on duty cycle, defined as the proportion of the integrated calcium concentration over the oscillation period, than on frequency alone. This demonstrates that NFAT acts primarily as a signal integrator of cumulative load rather than a frequency-selective decoder. This approach resolves a fundamental question in calcium encoding and demonstrates the value of optogenetics for isolating individual dynamical components of larger signaling behaviors.

Introduction:

Calcium-dependent transcription is a fundamental eukaryotic signaling mechanism that regulates critical functions in development, stress responses, and synaptic transmission (Clapham, 2007; Ghosh and Greenberg, 1995; Uhlen and Fritz, 2010; Uhlen et al., 2015).

Propagating waves of elevated calcium encode information in their waveform in order to coordinate these system-wide transcriptional programs within individual cells and across cell populations. The mechanism by which cells decode this information and incorporate it into their decision making processes remains unclear.

It is known that the transcriptional activity of calcium-dependent transcription factors is enhanced by increasing calcium oscillation frequency (Bito et al., 1997; Dolmetsch et al., 1997; Dolmetsch et al., 1998; Parekh, 2011; Salazar et al., 2008; Smedler and Uhlen, 2014; Tomida et al., 2003). However, cells decode oscillatory biochemical signals based on not only the peak amplitude and frequency as principle components of the waveform, but also the duty cycle (or duty ratio). Here, duty cycle is defined as cumulative load of calcium concentration elevated above basal levels with respect to time, normalized to a steady-state load of equal peak amplitude (Salazar et al., 2008). Oscillation duty cycle can serve as a measure of cumulative load that influences transcriptional signaling (Purvis and Lahav, 2013) (**Figure 1a).**

To understand whether cells decode each dynamical component of the calcium signal and initiate responses that are specific to those components, it is necessary to understand how frequency and duty cycle of calcium oscillations each affect transcription independently (Kalo and Shav-Tal, 2013; Schuster et al., 2002). However, experimental analyses tend to stimulate cells with fixed calcium pulse-widths, and under those conditions, frequency and duty cycle change concomitantly. Thus, it remains unclear whether calcium-dependent transcription factors primarily act as signal integrators of cumulative load delivered by pulsatile signals, or whether they selectively respond to specific oscillation frequencies. In principle, these "decoding principles" can be experimentally discerned by matching calcium duty cycle across frequencies, and vice versa, to respectively isolate the contributions frequency and duty cycle make to transcriptional activation levels.

Here, we use mathematical modeling, optogenetics, and synthetic biology to resolve the primary decoding principle for NFAT (Hogan et al., 2003), a calcium-dependent transcription

factor crucial to immune cell function, development, stem cell differentiation, and tumor progression (Horsley et al., 2008; Macian, 2005; Mancini and Toker, 2009; Nguyen and Di Giovanni, 2008). To activate NFAT, increases in cytoplasmic calcium concentration activate the calcium-dependent phosphatase, calcineurin (CN). Calcineurin, in turn, dephosphorylates cytoplasmic NFAT to expose its nuclear localization signal; dephophorylated (activated) NFAT then shuttles to the nucleus, binds its cognate promoter, and initiates transcription (**Figure 1a,** we call this nuclear translocation rate α). Activated NFAT is constitutively phosphorylated within the nucleus, and subsequently exported from it in a phosphorylation-dependent manner (we call the nuclear export rate β in Figure 1a). When cytoplasmic calcium levels fall, calcineurin activity decreases and the phosphorylated form of NFAT accumulates in the cytoplasm, halting NFAT-dependent transcription.

Because nuclear export is the rate-limiting step in returning NFAT activity to baseline (Colella et al., 2008; Kalo and Shav-Tal, 2013; Tomida et al., 2003; Yissachar et al., 2013), NFAT accumulates in the nucleus when the calcium oscillation frequency (we call this frequency ν in **Figure 1a**) exceeds export frequency (Salazar et al., 2008). Therefore, transcription under the NFAT promoter increases with increasing oscillation frequency, as originally demonstrated under duty cycle-unmatched conditions (Dolmetsch et al., 1997; Dolmetsch et al., 1998). However, NFAT may alternatively (or complementarily) integrate total elevated calcium concentrations, as originally proposed in a model of “integrative tracking” (Berridge, 2006; Berridge et al., 2003).

Results

Using a calcium decoding model with an analytic solution (Salazar et al., 2008), we performed a sensitivity analysis to identify the individual effect of specific parameters on the NFAT response. We calculated the mean NFAT transcriptional activity as a function of either

relative calcium oscillation frequency (ω) or duty ratio (γ) while holding the remaining components constant. The relative oscillation frequency is the determinant frequency parameter suggested by the model and is defined as oscillation frequency (ν) relative to NFAT nuclear export rate (β). This analysis (**Figure 1b**) spanned a physiological range of peak calcium amplitude (A) at either an optimal duty ratio or an optimal relative frequency (calculated using **Equations 1 and 2** in **Supplemental Procedures**).

This analysis revealed that frequency sensitivity over the physiologically relevant range (ω = 0-3) is confined to the lower range of relative frequency (ω < 1), with a maximum frequency-dependent enhancement of ~30% (**Figure 1b-i**). However, duty cycle has a more pronounced effect that spans the entire range of transcriptional activation regardless of oscillation amplitude **(Figure 1b-ii)**. The model thus suggests that NFAT is more sensitive to duty cycle than specific frequency and, consequently, is primarily an integrator of cumulative calcium load. Importantly, the analysis also informed our experimental design by identifying the parameter regimes in which the NFAT response is most sensitive to, as well as estimating the maximum change in NFAT activity as a function of these individual parameters.

Next, we tested these analytic results directly by optogenetically controlling intracellular calcium in HeLa cells, as described below (**Figures 1c** and **1d**), and correlating the oscillation waveforms to transcriptional activity in multi-plexed gene expression assays. Based on a mammalian synthetic optogenetic transcription device (Ye et al., 2011), the engineered HeLa cells stably expressed human melanopsin (hOPN4), a light-gated $G\alpha_q$-coupled opsin useful for optogenetic control of store-operated release of calcium from the endoplasmic reticulum (ER) (Lin et al., 2008; Provencio et al., 1998; Qiu et al., 2005). Calcium release drove luciferase reporter expression under the regulation of the NFAT promoter. HeLa cells were chosen because they primarily express one isoform (NFAT4, (Schaab et al., 2012)) that dominates the

frequency sensitivity (refer to **Supplemental Figure S1a** and **S1b**), thereby simplifying modeling and model-to-data correlations.

Calcium waveforms in individual cells were evoked by optical stimulation and measured via calcium imaging with X-Rhod-1. We identified stimulation conditions that yielded calcium transients of identical peak concentrations (amplitudes) while varying areas-under-the-curve (AUCs) (**Figure 2a**). Figure 2a shows the three waveforms and the empirically derived optical pulse-trains to reliably generate them. Repeated short pulses (1s-long every 5s, blue dots in **Figures 2a**) were used to prevent photoreceptor bleaching by constant illumination. Transcriptional induction epochs are created by repeating individual calcium transients and adjusting the inter-peak period in order to either match duty cycle across varying frequencies or match frequency across varying duty cycles (**Figure 2**). The highest oscillation frequency that allows calcium elevation to completely decay to the baseline was $\nu \sim 8$ mHz, and thus, optogenetic calcium clamping had sufficient temporal precision to ensure NFAT nuclear accumulation. The matching peak amplitudes (~0.27μM) exceed the half-saturation concentration for NFAT activation (K_s = 0.2μM, **Supplemental Figure S1c**).

To isolate the specific contribution of frequency on NFAT transcriptional activity, we matched the duty ratio by adjusting the period between repeated peaks from Figure 2a. Two frequency windows of interest (1.65 - 5 and 0.70 - 2.1 mHz) encompassed the most frequency-sensitive regime (ω = 0.3 - 1.0, **Figure 1b-i**), based on reported $1/\beta_{NFAT4}$ of 3.0 - 7.6 minutes (Kar and Parekh, 2015; Yissachar et al., 2013). Multiplexed transcription studies were performed in 24-well plates using custom illuminators that reproduce the calcium imaging conditions, for both melanopsin stimulation and X-Rhod-1 excitation, by controlling light-emitting diodes (LEDs) via potentiometers (irradiance) and microcontrollers (timing) (**Figures 2b-d**). No statistically significant difference in transcriptional activity was observed within either duty cycle-matched window (**Figure 2e**). Note that to limit cell variation and basal luciferase expression,

all data within a particular frequency window were collected simultaneously, but the two distinct frequency windows draw from different cell passages. The duty cycle-matched assays suggest that NFAT is not primarily a frequency-selective decoder of calcium oscillations, as initially proposed by others (Dolmetsch et al., 1997; Dolmetsch et al., 1998).

To determine whether NFAT is instead primarily an integrator of cumulative load, we assessed the effect of duty cycle on transcriptional activity, at fixed frequency and amplitude (**Figure 2f**). All data in Figure 2f were acquired simultaneously, but the frequency-matched dataset was generated with different cell passages than the duty cycle-matched one. The same waveforms in Figure 2a were used to span a three-fold duty cycle range in a regime (γ = 0.1 - 0.3) chosen to maximize sensitivity based on the model in Figure 1b-ii. Statistically significant differences were observed across this range. Similar-fold increases in cumulative load are sufficient to fundamentally alter cellular dynamics, including transitions between poised and actively proliferating stem cell states (Deng et al., 2015). The increased sensitivity to duty cycle over spike timing suggests that NFAT behaves as a signal integrator, as suggested by the mathematical model and hypothesized by others (Berridge, 2006; Berridge et al., 2003; Colella et al., 2008; Kar et al., 2012). Importantly, previous studies using paired pulses of calcium in rat basophilic leukemia cells (RBL) confirmed that NFAT activation indeed integrates calcium elevations that are coincident within an inter-pulse temporal cutoff (Kar et al., 2012). The results here reveal that such decoding-by-integration is in fact the dominant mechanism for NFAT.

The finding is also consistent with related studies on NFκB in immune cells (Song et al., 2012; Zhu et al., 2011) and the stimulus duration-dependent switching of CREB in neurons (Bito et al., 1996, 1997), thus suggesting that decoding-by-integration is a general transcriptional principle applicable to many mammalian calcium-responsive activators. However, because these transcription factors differ from NFAT in terms of the presence of negative feedback loops mediated by IκB in NFκB signaling (Levine et al., 2013; Tay et al., 2010) and in terms CREB

responsiveness to additional second messenger beyond calcium (Shaywitz and Greenberg, 1999), one should keep attuned to signaling network-specific differences in the decoding principles employed by different calcium-dependent transcription factors.

Discussion

Systematically isolating the contributions of individual waveform parameters to calcium-dependent transcriptional activity clarifies the role of frequency in studies performed with steady-state loads and/or unmatched duty cycles. Previously observed enhancements with shortening periods were likely attributable to consequent differences in cumulative load. This distinction does not imply frequency insensitivity, since excited cells typically increase their calcium spike frequency (Schuster et al., 2002), but rather shifts the attributable source of enhancement to better reflect the decoding principle, from specific frequency or peak timing, to frequency-coupled cumulative load.

NFAT signaling relies on pulsatile calcium to coordinate with other regulators to direct diverse signaling outputs (Purvis and Lahav, 2013), and to achieve selectivity by temporal cutoff filtering (of isoform-specific translocation rates (Levine et al., 2013; Yissachar et al., 2013)), in addition to distinct spatial calcium signatures within cells (Di Capite et al., 2009; Kar and Parekh, 2015; Mehta et al., 2014; Parekh, 2011). Single-cell studies on calcium-dependent transcription factors have shown that nuclear translocation occurs in pulsatile bursts of increasing output frequency with increasing steady-state calcium input (Cai et al., 2008; Kar and Parekh, 2015; Levine et al., 2013; Tay et al., 2010; Yissachar et al., 2013), so that coordinated gene expression under one promoter depends on the fraction of localization time but not exact timing or true frequency (frequency-modulated (FM) coordination, (Cai et al., 2008; Levine et al., 2013)). Since fraction of localization time is also a duty ratio, the optogenetic findings here are

consistent with the general FM-coordination principle, but now applied to the upstream, non-steady-state oscillatory input.

In total, this work defines a workflow for using mathematical modeling, optogenetics, and mammalian synthetic biology to isolate the decoding principles at work in dynamical regulation of transcription. By resolving this experimental confound in interpreting the roles of interdependent components of an oscillatory signal, this parameterized analysis refines a key decoding principle of frequency modulated calcium-dependent transcription to better explain how mammalian cells dynamically respond to complex stimuli.

Experimental Procedures: A brief summary of experimental procedures is provided below (refer to **Supplemental Information 1** for detailed procedures).

[Genetic constructs and transduction]: Clonal populations of HeLa cell lines stably expressing human melanopsin (hOPN4) were created by lentiviral transduction under the CMV promoter. For transcriptional activation assays, cells were transfected with NFAT-luciferase reporter plasmid pGL4.30[luc2P/NFAT-RE/Hygro] (Promega E8481) using TransIT-LT1 transfection agent (Mirus Biotech) according to manufacturer protocols. Cells were plated on 1cm coverslips for calcium imaging or black 24-well plates for gene expression assays, with collagen adhesion layers.

[Calcium imaging]: Calcium imaging with X-Rhod-1 (Invitrogen X-14210) in phenol-free media was performed on a Leica DMI6000B fluorescence microscope (Chroma filters, λ_{ex} < 575nm and λ_{em} > 580nm), equipped with Metamorph software for automated optical stimulation (Lumencor LEDs, hOPN4 activation: λ = 470nm @ 3.8mW/cm^2, X-Rhod-1 imaging: λ = 570nm @ 2.8mW/cm^2), fluorescence imaging (pco.edge sCMOS camera), and fluid perfusion (Harvard Apparatus syringe pump and Autom-8 perfusion chamber). Absolute calcium concentrations of individual cells were quantified by perfusing calcium ionophore (Sigma-Aldrich C7522), and

calcium-free (F_{min}) and high calcium calibration (F_{max}) buffers immediately after measuring optogenetically induced calcium transients and employing a calcium calibration standard (characterized in Supplemental Information**,** Section 7: Calcium calibration) for fluorescence-calcium conversion (refer to Supplemental Information**,** Section 6: Calcium imaging). Image processing, cell segmentation, and measurements of fluorescence intensity of individual cells were performed using ImageJ and Metamorph. Mean AUC and peaks reported in Figure 2a are the average of all single-cell traces from 6 coverslips (3 epochs per cell, 306-490 cells in total).

[Gene expression assays]: LED illuminators on custom circuit boards for optogenetic induction of luciferase reporter expression were aligned to 24-well plates (black-walled to prevent optogenetic cross-talk between wells). Optical stimulation conditions between gene expression assays and calcium imaging were matched via (i) an Arduino microcontroller to control LED timing and (ii) variable potentiometers to tune LED irradiance (hOPN4 activation: λ = 470nm @ 3.8mW/cm^2, X-Rhod-1 imaging: λ = 570nm @ 2.8mW/cm^2). Cells were optogenetically stimulated for 6 hours in phenol-free media (Clontech) and chemically lysed with cell culture lysis reagent. Luciferase bioluminescence was quantified on a Tecan M200 plate reader according to assay manufacturer protocols (Promega E1501), and normalized to non-illuminated wells from the same plate. Refer to Supplemental Information Section 11: Illuminator construction and programming for schematics. Refer to Supplemental File 1 for downloadable CAD files.

[Mathematical modeling and data analyses]: Mathematical modeling and sensitivity analysis were performed using MATLAB. Data was analyzed in MATLAB and plotted in R and Excel. Statistical analyses were performed in R.

Supplemental Information:

Supplemental Information 1: Detailed experimental procedures and supplemental data, including: Supplemental Figure 1: (a) Model of calcium-induced NFAT nuclear shuttling; (b) Isoform specific analysis of NFAT transcriptional activation sensitivity to calcium oscillation frequencies; (c) Supplemental Figure 3: NFAT transcriptional activation as a function of steady-state calcium concentration; Supplemental Figure 2: CAD schematics of custom illuminator for multiplexed optogenetic transcriptional induction.

Author Contributions: PH and BYC conceived of all experiments, conducted all data analysis, and wrote the paper. PH performed all experiments.

Acknowledgments: The authors thank Arjun Raj, David Issadore, Ed Boyden, Daniel Schmidt, and the members of the Chow Lab for helpful discussion. The authors also thank the Boyden Lab (MIT) for the hOPN4 plasmid, and the following laboratories at Penn for generously sharing reagents, cell lines, and equipment: Cremins, Gadue, Issadore, Lazarra, Meaney, and Raj. BYC acknowledges the support of NSF Biophotonics (CBET 126497), W.W. Smith Charitable Trust for the Heart, Penn Medicine Neuroscience Center, NIH/NIDA (1R21 DA040434-01), and DARPA (Living Foundries HR0011-12-C-0068). PH is on partial fellowship support from the Thai Ministry of Science and Technology Scholarship. The authors declare no conflicts of interest.

Figure and Table Legends:

Figure 1. Calcium decoding by the NFAT transcription factor. (A) NFAT information processing principles. *(Left)* Calcium oscillations encode information in their frequency, peak

amplitude, and duty ratio. *(Middle)* Elevated calcium induces NFAT translocation and transcriptional activation at rate α. Nuclear export at rate β deactivates transcriptional signaling (NFAT, inactive form; NFAT*, active form). *(Right)* Calcium signal processing is frequency-selective when transcription is enhanced at specific oscillation frequencies (absolute ν, or relative $\omega = \nu/\beta$). Alternatively, NFAT is a signal integrator if the enhancement is attributable to duty ratio. **(B)** Mathematical models of NFAT sensitivity to *(i)* calcium frequency and *(ii)* duty ratio suggest it is primarily an integrator of cumulative calcium delivered by pulsatile loads regardless of peak amplitude, as the duty ratio-response spans the whole activation range whereas frequency dependence is more modest. Note that the models for 0.5 and 1.0 μM calcium overlap. **(C)** Signaling pathways and genetic circuit diagram of a synthetic optogenetic transcription device for decoding calcium encoding in HeLa cells. Calcium oscillations are optically created by melanopsin-mediated store-operated release, activating NFAT via calcineurin (CN). Transcriptional activity of the specific oscillation is reported by luciferase under the NFAT promoter. **(D)** Confocal micrograph of engineered HeLa cells stably expressing melanopsin, visualized by a C-terminal GFP tag.

Figure 2. Parametric analysis of calcium oscillation frequency and duty cycle on NFAT transcriptional signaling. (A) Calcium transients of identical peak amplitude but varying area-under-the-curve (AUC) (presented as Rel. AUC, relative to the AUC of 0.5s-stimulation) created by melanopsin stimulation, as measured by calcium indicator X-Rhod-1 imaging. Colored dots represent optical stimulation pulses. Data are represented as mean ± SEM (with 306-490 cells per averaged trace). **(B)** Schematic of custom illuminator to deliver identical stimulation as used in calcium imaging experiments, using a variable potentiometer and microcontroller to respectively tune irradiance and control timing per row of LEDs (see also Supplemental Figure S2). **(C)** Schematic for multiplexed optogenetic transcription assays in a multi-well plate (Blue

illuminator, melanopsin stimulation; yellow illuminator, recapitulation of X-Rhod-1 imaging). **(D)** Photograph of the experimental setup, here shown outside of the tissue culture incubator. **(E)** Isolating the role of calcium frequency on NFAT transcriptional activity by optogenetic duty-cycle matching at fixed peak amplitude. Luciferase reporter expression under the transcriptional regulation of NFAT is optogenetically induced by melanopsin stimulation (refer to Figure 1c). Transcriptional activity is normalized to non-illuminated cells that are otherwise identical. No statistically significant difference is observed between frequencies at a given duty ratio (unpaired t-test). **(F)** Isolating the role of duty cycle under frequency-matched conditions at fixed peak amplitude. Transcriptional activity increases with duty ratio with statistical significance (unpaired t-test, * = $p < 0.05$, *** = $p < 0.001$), suggesting that NFAT is primarily an integrator of cumulative load. In (E-F), data are represented as mean ± SD.

References:

Berridge, M.J. (2006). Remodelling Ca2+ signalling systems and cardiac hypertrophy. Biochem Soc Trans *34*, 228-231.

Berridge, M.J., Bootman, M.D., and Roderick, H.L. (2003). Calcium signalling: dynamics, homeostasis and remodelling. Nat Rev Mol Cell Biol *4*, 517-529.

Bito, H., Deisseroth, K., and Tsien, R.W. (1996). CREB phosphorylation and dephosphorylation: a Ca(2+)- and stimulus duration-dependent switch for hippocampal gene expression. Cell *87*, 1203-1214.

Bito, H., Deisseroth, K., and Tsien, R.W. (1997). Ca2+-dependent regulation in neuronal gene expression. Current opinion in neurobiology *7*, 419-429.

Cai, L., Dalal, C.K., and Elowitz, M.B. (2008). Frequency-modulated nuclear localization bursts coordinate gene regulation. Nature *455*, 485-490.

Clapham, D.E. (2007). Calcium Signaling. Cell *131*, 1047-1058.

Colella, M., Grisan, F., Robert, V., Turner, J.D., Thomas, A.P., and Pozzan, T. (2008). Ca2+ oscillation frequency decoding in cardiac cell hypertrophy: role of calcineurin/NFAT as Ca2+ signal integrators. Proceedings of the National Academy of Sciences of the United States of America *105*, 2859-2864.

Deng, H., Gerencser, A.A., and Jasper, H. (2015). Signal integration by Ca2+ regulates intestinal stem-cell activity. Nature *528*, 212-217.

Di Capite, J., Ng, S.W., and Parekh, A.B. (2009). Decoding of Cytoplasmic Ca2+ Oscillations through the Spatial Signature Drives Gene Expression. Current Biology *19*, 853-858.

Dolmetsch, R.E., Lewis, R.S., Goodnow, C.C., and Healy, J.I. (1997). Differential activation of transcription factors induced by Ca2+ response amplitude and duration. Nature *386*, 855-858.

Dolmetsch, R.E., Xu, K., and Lewis, R.S. (1998). Calcium oscillations increase the efficiency and specificity of gene expression. Nature *392*, 933-936.

Ghosh, A., and Greenberg, M.E. (1995). Calcium signaling in neurons: molecular mechanisms and cellular consequences. Science *268*, 239-247.

Hogan, P.G., Chen, L., Nardone, J., and Rao, A. (2003). Transcriptional regulation by calcium, calcineurin, and NFAT. Genes & development *17*, 2205-2232.

Horsley, V., Aliprantis, A.O., Polak, L., Glimcher, L.H., and Fuchs, E. (2008). NFATc1 Balances Quiescence and Proliferation of Skin Stem Cells. Cell *132*, 299-310.

Kalo, A., and Shav-Tal, Y. (2013). Acting on impulse: dissecting the dynamics of the NFAT transcriptional response. Genome Biology *14*, 102-102.

Kar, P., Nelson, C., and Parekh, Anant B. (2012). CRAC Channels Drive Digital Activation and Provide Analog Control and Synergy to Ca2+-Dependent Gene Regulation. Current Biology *22*, 242-247.

Kar, P., and Parekh, Anant B. (2015). Distinct Spatial Ca2+ Signatures Selectively Activate Different NFAT Transcription Factor Isoforms. Molecular Cell *58*, 232-243.

Levine, J.H., Lin, Y., and Elowitz, M.B. (2013). Functional roles of pulsing in genetic circuits. Science *342*, 1193-1200.

Lin, B., Koizumi, A., Tanaka, N., Panda, S., and Masland, R.H. (2008). Restoration of visual function in retinal degeneration mice by ectopic expression of melanopsin. Proceedings of the National Academy of Sciences of the United States of America *105*, 16009-16014.

Macian, F. (2005). NFAT proteins: key regulators of T-cell development and function. Nat Rev Immunol *5*, 472-484.

Mancini, M., and Toker, A. (2009). NFAT Proteins: Emerging Roles in Cancer Progression. Nature reviews Cancer *9*, 810-820.

Mehta, S., Aye-Han, N.-N., Ganesan, A., Oldach, L., Gorshkov, K., and Zhang, J. (2014). Calmodulin-controlled spatial decoding of oscillatory Ca(2+) signals by calcineurin. eLife *3*, e03765.

Nguyen, T., and Di Giovanni, S. (2008). NFAT signaling in neural development and axon growth. International journal of developmental neuroscience : the official journal of the International Society for Developmental Neuroscience *26*, 141-145.

Parekh, A.B. (2011). Decoding cytosolic Ca2+ oscillations. Trends in biochemical sciences *36*, 78-87.

Provencio, I., Jiang, G., De Grip, W.J., Hayes, W.P., and Rollag, M.D. (1998). Melanopsin: An opsin in melanophores, brain, and eye. Proceedings of the National Academy of Sciences of the United States of America *95*, 340-345.

Purvis, Jeremy E., and Lahav, G. (2013). Encoding and Decoding Cellular Information through Signaling Dynamics. Cell *152*, 945-956.

Qiu, X., Kumbalasiri, T., Carlson, S.M., Wong, K.Y., Krishna, V., Provencio, I., and Berson, D.M. (2005). Induction of photosensitivity by heterologous expression of melanopsin. Nature *433*, 745-749.

Salazar, C., Politi, A.Z., and Höfer, T. (2008). Decoding of Calcium Oscillations by Phosphorylation Cycles: Analytic Results. Biophysical Journal *94*, 1203-1215.

Schaab, C., Geiger, T., Stoehr, G., Cox, J., and Mann, M. (2012). Analysis of High Accuracy, Quantitative Proteomics Data in the MaxQB Database. Molecular & Cellular Proteomics *11*.

Schuster, S., Marhl, M., and Höfer, T. (2002). Modelling of simple and complex calcium oscillations. European Journal of Biochemistry *269*, 1333-1355.

Shaywitz, A.J., and Greenberg, M.E. (1999). CREB: a stimulus-induced transcription factor activated by a diverse array of extracellular signals. Annu Rev Biochem *68*, 821-861.

Smedler, E., and Uhlen, P. (2014). Frequency decoding of calcium oscillations. Biochim Biophys Acta *1840*, 964-969.

Song, S., Li, J., Zhu, L., Cai, L., Xu, Q., Ling, C., Su, Y., and Hu, Q. (2012). Irregular Ca(2+) oscillations regulate transcription via cumulative spike duration and spike amplitude. The Journal of biological chemistry *287*, 40246-40255.

Tay, S., Hughey, J.J., Lee, T.K., Lipniacki, T., Quake, S.R., and Covert, M.W. (2010). Single-cell NF-kappaB dynamics reveal digital activation and analogue information processing. Nature *466*, 267-271.

Tomida, T., Hirose K Fau - Takizawa, A., Takizawa A Fau - Shibasaki, F., Shibasaki F Fau - Iino, M., and Iino, M. (2003). NFAT functions as a working memory of Ca2+ signals in decoding Ca2+ oscillation. EMBO J *22*, 3825-3832
.

Uhlen, P., and Fritz, N. (2010). Biochemistry of calcium oscillations. Biochemical and biophysical research communications *396*, 28-32.

Uhlen, P., Fritz, N., Smedler, E., Malmersjo, S., and Kanatani, S. (2015). Calcium signaling in neocortical development. Developmental neurobiology *75*, 360-368.

Ye, H., Baba, M.D.-E., Peng, R.-W., and Fussenegger, M. (2011). A Synthetic Optogenetic Transcription Device Enhances Blood-Glucose Homeostasis in Mice. Science *332*, 1565-1568.

Yissachar, N., Sharar Fischler, T., Cohen, A.A., Reich-Zeliger, S., Russ, D., Shifrut, E., Porat, Z., and Friedman, N. (2013). Dynamic response diversity of NFAT isoforms in individual living cells. Mol Cell *49*, 322-330.

Zhu, L., Song, S., Pi, Y., Yu, Y., She, W., Ye, H., Su, Y., and Hu, Q. (2011). Cumulated Ca2(+) spike duration underlies Ca2(+) oscillation frequency-regulated NFkappaB transcriptional activity. J Cell Sci *124*, 2591-2601.

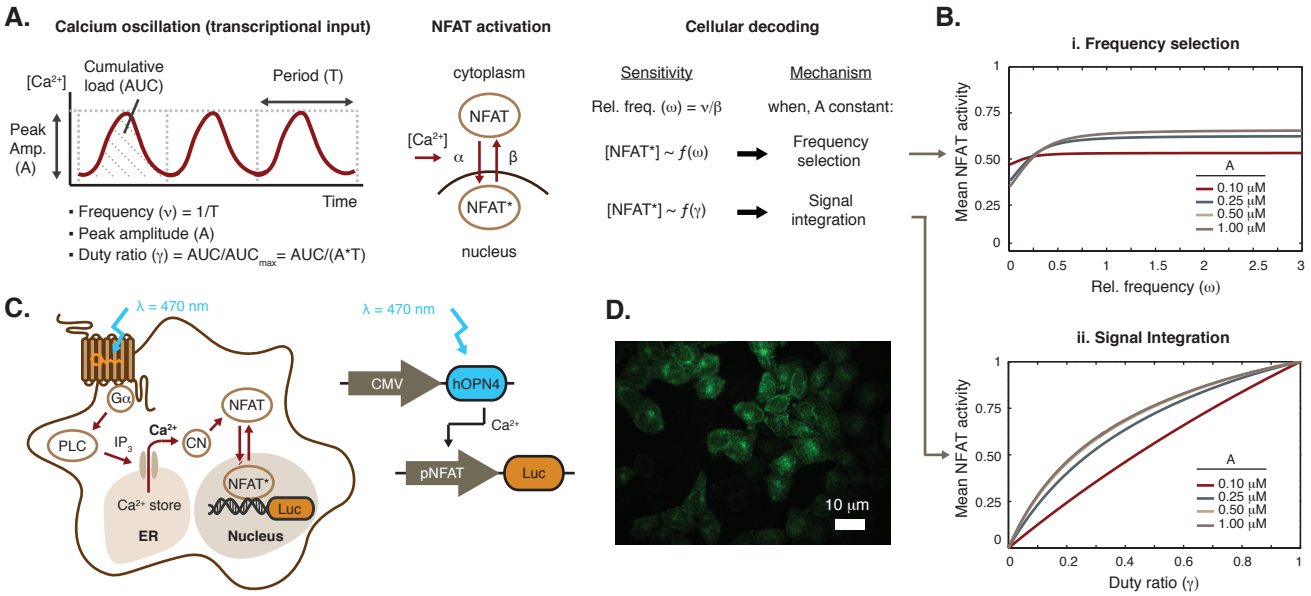

Figure 1. Calcium decoding by the NFAT transcription factor. (A) NFAT information processing principles. *(Left)* Calcium oscillations encode information in their frequency, peak amplitude, and duty ratio. *(Middle)* Elevated calcium induces NFAT translocation and transcriptional activation at rate α. Nuclear export at rate β deactivates transcriptional signaling (NFAT, inactive form; NFAT*, active form). *(Right)* Calcium signal processing is frequency-selective when transcription is enhanced at specific oscillation frequencies (absolute ν, or relative ω = ν/β). Alternatively, NFAT is a signal integrator if the enhancement is attributable to duty ratio. **(B)** Mathematical models of NFAT sensitivity to *(i)* calcium frequency and *(ii)* duty ratio suggest it is primarily an integrator of cumulative calcium delivered by pulsatile loads regardless of peak amplitude, as the duty ratio-response spans the whole activation range whereas frequency dependence is more modest. Note that the models for 0.5 and 1.0 μM calcium overlap. **(C)** Signaling pathways and genetic circuit diagram of a synthetic optogenetic transcription device for decoding calcium encoding in HeLa cells. Calcium oscillations are optically created by melanopsin-mediated store-operated release, activating NFAT via calcineurin (CN). Transcriptional activity of the specific oscillation is reported by luciferase under the NFAT promoter. **(D)** Confocal micrograph of engineered HeLa cells stably expressing melanopsin, visualized by a C-terminal GFP tag.

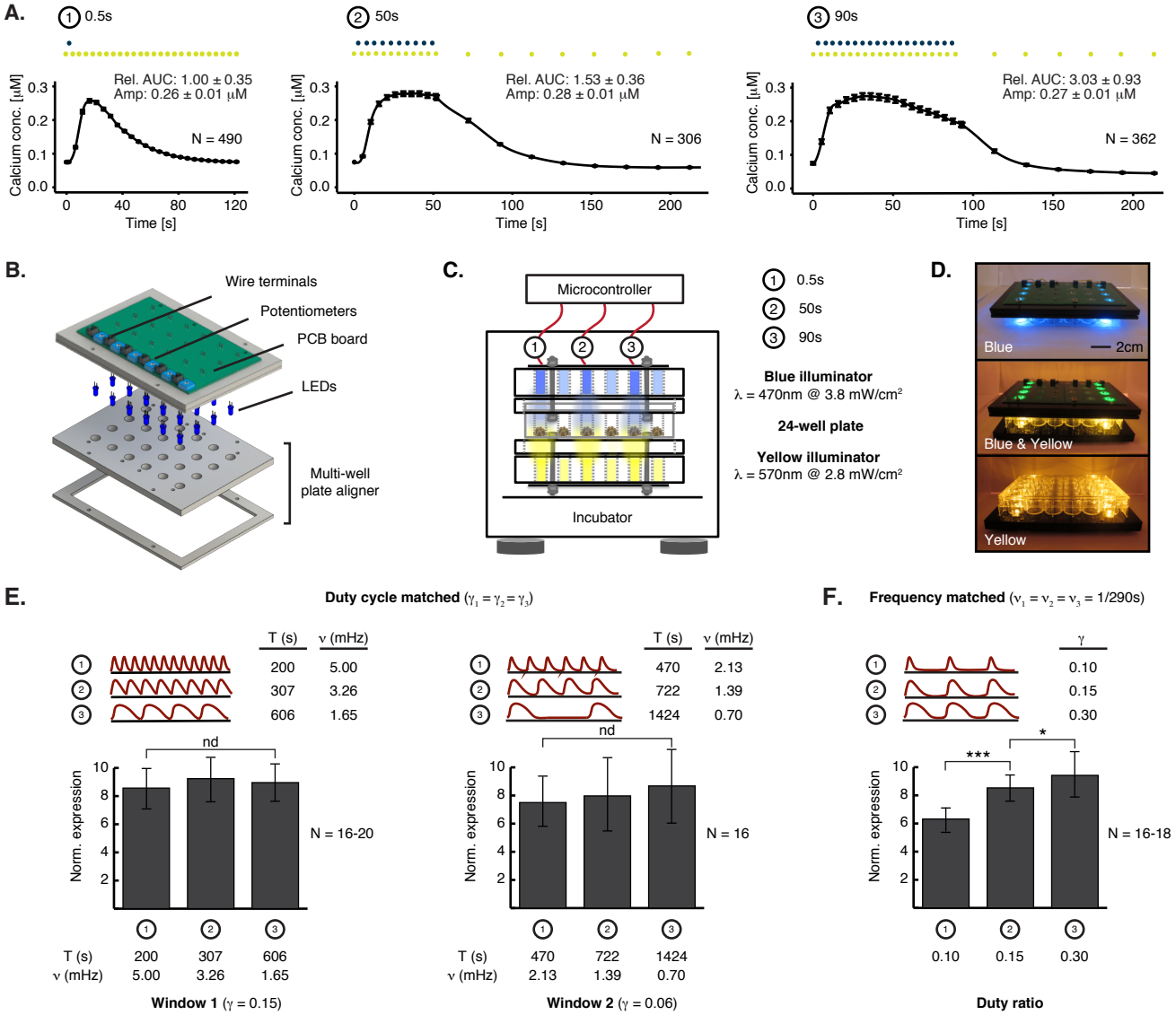

Figure 2. Parametric analysis of calcium oscillation frequency and duty cycle on NFAT transcriptional signaling. (A) Calcium transients of identical peak amplitude but varying area-under-the-curve (AUC) (presented as Rel. AUC, relative to the AUC of 0.5s-stimulation) created by melanopsin stimulation, as measured by calcium indicator X-Rhod-1 imaging. Colored dots represent optical stimulation pulses. Data are represented as mean ± SEM (with 306-490 cells per averaged trace). **(B)** Schematic of custom illuminator to deliver identical stimulation as used in calcium imaging experiments, using a variable potentiometer and microcontroller to respectively tune irradiance and control timing per row of LEDs (see also Figure S4). **(C)** Schematic for multiplexed optogenetic transcription assays in a multi-well plate (Blue illuminator, melanopsin stimulation; yellow illuminator, recapitulation of X-Rhod-1 imaging). **(D)** Photograph of the experimental setup, here shown outside of the tissue culture incubator. **(E)** Isolating the role of calcium frequency on NFAT transcriptional activity by optogenetic duty-cycle matching at fixed peak amplitude. Luciferase reporter expression under the transcriptional regulation of NFAT is optogenetically induced by melanopsin stimulation (refer to Figure 1c). Transcriptional activity is normalized to non-illuminated cells that are otherwise identical. No statistically significant difference is observed between frequencies at a given duty ratio (unpaired t-test). **(F)** Isolating the role of duty cycle under frequency-matched conditions at fixed peak amplitude. Transcriptional activity increases with duty ratio with statistical significance (unpaired t-test, * = $p < 0.05$, *** = $p < 0.001$), suggesting that NFAT is primarily an integrator of cumulative load. In (E-F), data are represented as mean ± SD.

Document S1. Supplemental Figures and Procedures

A. Supplemental Figures

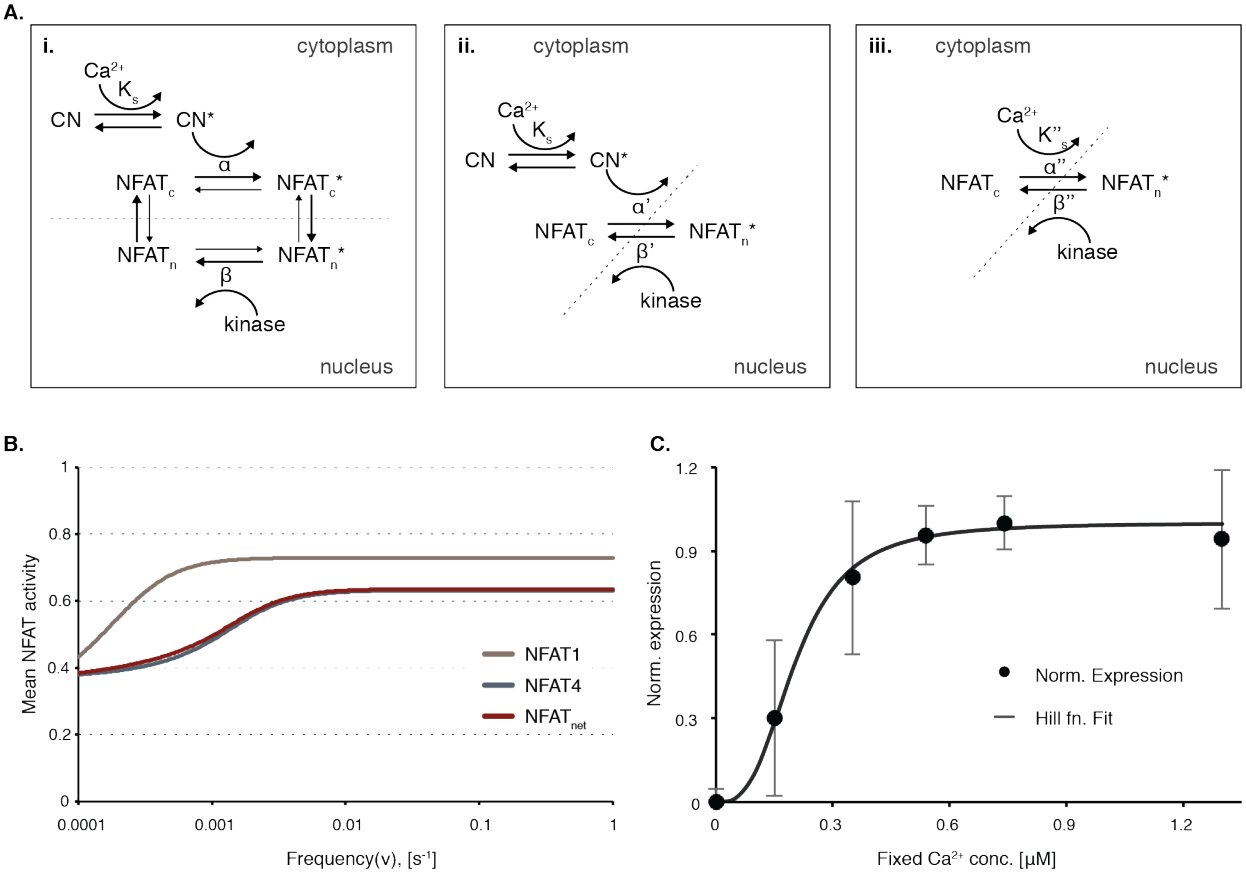

Figure S1. Model development to describe NFAT transcriptional activity by calcium oscillations. (A) *(Related to Figure 1B)* Model of calcium-induced NFAT nuclear shuttling. **(i)** Model in which NFAT de/re-phosphorylation is separated from a nuclear import/export. **(ii)** Simplified model in which de/re-phosphorylation is lumped with translocation as an activation/deactivation step. **(iii)** Minimal model assuming fast calcium-calcineurin binding and steady-state calcineurin (CN) concentrations, which was used to analyze the sensitivity of NFAT activity to frequency and duty ratio. **(B)** *(Related to Figures 1B-D)* Isoform specific and isoform weighted-average NFAT activation sensitivity to a physiological range of calcium oscillation frequencies. The net NFAT activity or expression-weighted average activity of the NFAT1 and NFAT4 isoforms found in HeLa cells resembles the activity of NFAT4, suggesting that the frequency sensitive-response is dominated by NFAT4. **(C)** *(Related to Figure 2A)* NFAT transcriptional activity as a function of steady-state calcium concentration in engineered melanopsin-HeLa cells**,** assessed by first fixing or clamping calcium concentration in the dark, and then quantifying the expression of luciferase under the NFAT promoter (normalized, ± s.d.).

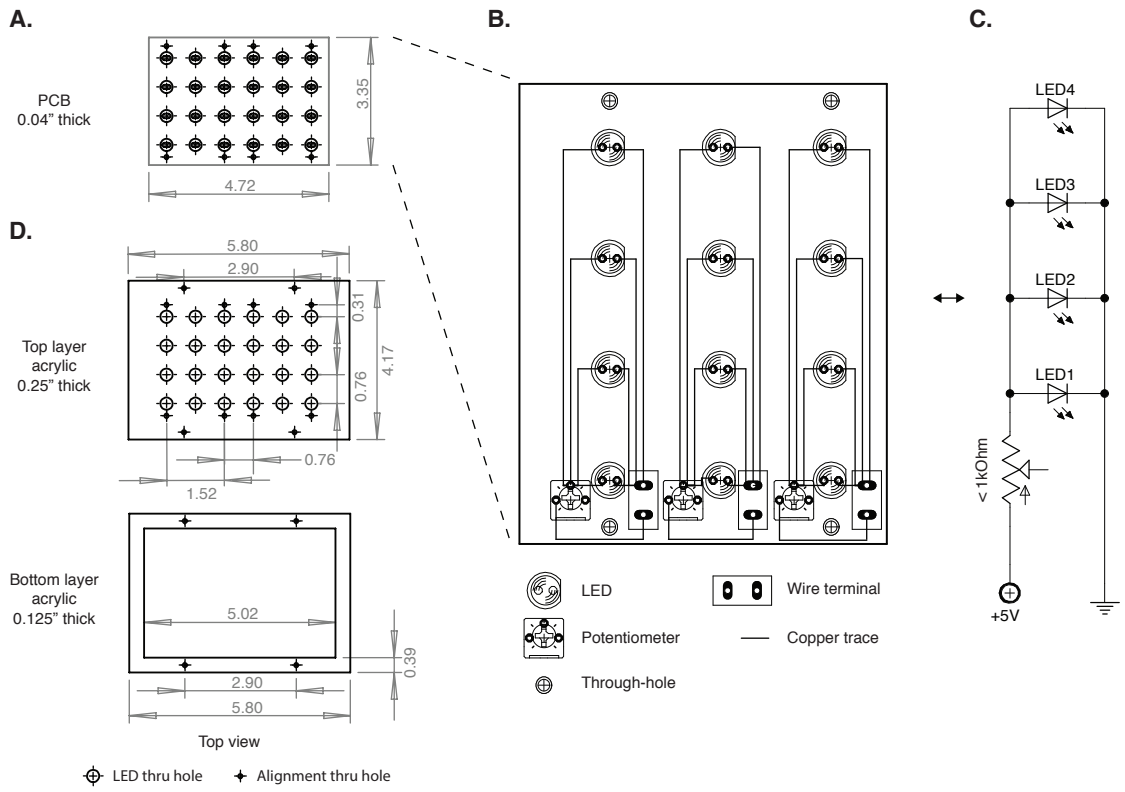

Figure S2. *(Refer to Figure 2B)* **CAD schematics of custom illuminator for multiplexed optogenetic transcriptional induction** (scale in inches). **(A)** Top view of PCB with six independent columns of LEDs per 24-well plate. **(B)** PCB layout with 3 columns shown. Each column contains four LEDs connected in parallel with a 1kΩ variable potentiometer, and a wire terminal. **(C)** Circuit diagram of a single LED column on the PCB. **(D)** Top view of acrylic positioning plates.

B. Supplemental Procedures

1. Mathematical modeling of NFAT signaling

Increases in calcium signal activate phosphatase calcineurin (CN), which in turn binds and dephosphorylates cytoplasmic NFAT, exposing its nuclear localization signal for nuclear translocation and transcriptional initiation. Nuclear NFAT is re-phosphorylated by kinases resulting in translocation back to cytoplasm (**Figure S1A-i**). The de-phosphorylation and nuclear import of NFAT can be lumped into one step and described as NFAT activation, and likewise re-phosphorylation and nuclear export of NFAT can be lumped as an inactivation step (**Figure S1A-ii**). Because calcium-calcineurin binding is generally much faster than NFAT de-phosphorylation, we assume steady-state CN levels, yielding the simplified model (shown in **Figure S1A-iii** and main text Figure 1).

To derive an analytical solution for average NFAT activity in response to oscillatory calcium, the oscillation is modeled as a square-wave (Salazar et al., 2008), and average or mean NFAT activity as time approaches infinity is described as ($\overline{X}$):

$$\overline{X} = \gamma + \left[\frac{\omega\sigma}{1+\sigma}\cdot\frac{(1-e^{-\gamma(1+\sigma)/\omega})(1-e^{-(1-\gamma)/\omega})}{1-e^{-(1+\gamma\sigma)/\omega}}\right], \quad \text{where} \qquad \textbf{Equation 1a}$$

$$\text{The effective activation rate: } \sigma = \frac{\alpha''}{\beta''}\cdot\frac{(A/K''_s)^n}{1+(A/K''_s)^n} \qquad \textbf{Equation 1b}$$

$$\text{Relative oscillation frequency: } \omega = \frac{1}{\beta'' T} \qquad \textbf{Equation 1c}$$

$$\text{Duty ratio: } \gamma = \frac{\Delta}{T} \qquad \textbf{Equation 1d}$$

A, T, and Δ are calcium peak amplitude, period, and spike width, respectively. NFAT half-saturation constant and Hill coefficient were identified experimentally as described in Section 10, and the import rate (α) and the export rate (β) were obtained from experimental reports (Kar and Parekh, 2015; Yissachar et al., 2013). Apostrophe superscripts in Equation 1 are used to refer to the model depicted in Figure S1A-iii, and with in the main text, α = α", β = β", and $K_s = K_s$".

2. Sensitivity analysis

NFAT sensitivity to relative frequency was evaluated using Equation 1, with ω spanning 0 to 3. The sensitivity is high at low duty ratios, and maximized at an optimal duty ratio of (Salazar et al. 2008):

$$\gamma_{opt} = \frac{\sqrt{1+\sigma}-1}{\sigma}. \qquad \textbf{Equation 2}$$

Figure 1B of the main text was generated at the optimal duty ratio. The sensitivity also increases with the oscillation amplitude and saturates at A = 0.5. NFAT sensitivity to duty ratio was evaluated with ω = 1, where the transcriptional activity is saturated based on the results of the aforementioned sensitivity analysis to relative frequency (Refer to Figure 1B of main text).

As previously suggested (Yissachar et al., 2013), different NFAT isoforms exhibit distinct nuclear translocation kinetics. To evaluate the total NFAT activity averaged over the isoform repertoire, weighted sensitivity analysis was also performed using a reported isoform expression ratio in HeLa cells of 0.83 $\log_{10}$(ppm) NFAT1 vs. 2.0 $\log_{10}$(ppm) NFAT4 (Schaab et al., 2012). The net NFAT sensitivity (**Figure S1B**) is relatively similar to that of NFAT4, suggesting that the frequency response in HeLa cells is dominated by NFAT4, and thus for simplicity, use the export rate of NFAT4 as the lump export rate in our system. The average NFAT activity was calculated over the entire duty ratio range and plotted in main text Figure 1B with a relative frequency of 1. The sensitivity changes only slightly with relative frequency, while increased amplitude enhances sensitivity at low duty ratios.

3. Genetic constructs

The pLJM1-melanopsin-GFP plasmid was constructed by subcloning human melanopsin (hOPN4, provided by the Boyden Lab, MIT) fused to a C-terminal EGFP reporter with an enhanced-trafficking signal between the NheI and EcoRI restriction sites of lentiviral vector pLJM1-EGFP (provided by the Gadue Lab, Penn). The plasmid was propagated in NEB Stable cells, and purified using a QIAGEN plasmid maxi kit to generate lentivirus. The NFAT luciferase reporter plasmid pGL4.30[luc2P/NFAT-RE/Hygro] (Promega E8481) was propagated in DH5α cells, and purified using QIAGEN plasmid maxi kit (Qiagen 12165). Unless stated otherwise, all oligonucleotides were synthesized by IDT and cloning was sequence verified by Sanger sequencing (Penn Cell Center).

4. Cell culture

HeLa cells (provided by the Raj Lab, Penn) were grown in Dulbecco's modified Eagle's medium (DMEM) with GlutaMAX (Invitrogen 10566016), supplemented with 10% heat-inactivated fetal bovine serum (FBS) (Seradigm 1500-500) and 1% Penicillin-Streptomycin (Invitrogen 15140122). Cells were maintained in a standard water-jacketed mammalian cell culture incubator (Thermo/Forma 3110).

5. Lentiviral generation of stable cell lines

To generate lentivirus, HEK293T cells (provided by the Lazzara Lab, Penn) were transfected with pLJM1-melanopsin-EGFP and 3rd generation packaging system plasmids (or helper plasmids). The media was replaced one day after transfection, and virus-containing supernatant was collected on the second and the third days. After centrifugation (1000 rpm, 5 minutes), the supernatant was filtered (0.4um PES) and used immediately or stored at 4°C for <7 days. HeLa cells were lentivirally infected and selected using 1 ug/ml Puromycin (Clontech 631305). Individual clones expressing melanopsin-EGFP were picked under a sterile fluorescence microscope (courtesy of the Cremins Lab, Penn) and grown in 24-well plates. Optogenetic performance or light-induced store operated release was assessed for each clone by calcium imaging (see **Section 6: Calcium imaging**), in order to select a suitable clone with high light responsiveness and minimal signal attenuation by repeated illuminations. Membrane localization was assessed by confocal microscopy (Leica SP5, courtesy of the Meaney Lab, Penn).

6. Calcium imaging

Calcium imaging was performed on an automated Leica DMI6000B fluorescence microscope (custom Chroma dichroic filter cube, λ_{ex} < 575nm and λ_{em} > 580nm), equipped with a sCMOS camera (pco.edge) and LED illuminator (Lumencor Spectra-X) for fluorescence imaging and optogenetic stimulation, all under Metamorph software control. Cells seeded on collagen-coated German glass coverslips (24 hours in advance) were incubated with 2μM X-Rhod-1 (Invitrogen X-14210) for 30 minutes at 37°C, and then washed and replaced with phenol-free CO_2-independent media (phenol-free HBSS supplemented with 1% L-glutamine, 1% Penn/Strep, 2% essential amino acids, 1% non-essential amino acids, 2.5% HEPES pH 7.0, and 10% serum), supplemented with 2μM all-trans retinal (Sigma-Aldrich R2500). After incubating cells for 30 minutes for dye de-esterification, the coverslip was transferred to a perfusion chamber (Autom8, with a Harvard Apparatus Syringe Pump) for imaging. It should be noted that genetically encoded calcium indicators were not employed because those with red-shifted excitation from melanopsin, such as RCaMP (Akerboom et al., 2013), required imaging irradiances that saturated melanopsin signaling despite the spectral separation, and bioluminescent indicators lacked sufficient temporal resolution in our hands (Saito et al., 2012).

Time-lapse images of dye-loaded cells were taken with 0.5s exposures on a 20x air objective (λ_{ex} = 570nm, 2.8mW/cm^2). Melanopsin stimulation paradigms (λ_{ex} = 470nm, 3.8mW/cm^2) were developed after scanning ranges of individual pulse duration (0.1 - 50s), pulse interval (1 - 5s), and total pulse train duration (1 – 90s). Stimulation epochs were repeated three times per imaging trial to assess for photoreceptor bleaching, and traces shown in main

text Figure 2A are derived from the average per trial. A single 0.5s pulse was sufficient to saturate the optogenetic store-operated release response, and the longer stimulation paradigms (50s and 90s) reported in main text were chosen such that the resulting period-adjusted calcium duty ratios were matched over a three-fold frequency range. Image processing, cell segmentation, and measurements of fluorescence intensity of individual cells were performed using ImageJ and Metamorph.

To convert relative fluorescence to absolute calcium concentration, minimum (F_{min}) and maximum fluorescence (F_{max}) signals were obtained immediately after imaging every cover slip, and then input into Equation 3 (refer to **Section 7: Calcium calibration**, below). To obtain F_{min}, cells were washed with calcium-free HBSS three times, and then were incubated with F_{min}-buffer for 10 minutes (HBSS, 5μM calcium ionophore [IM, Sigma-Aldrich C7522], and 3μM EGTA [Sigma-Aldrich E8145]) to allow complete EGTA sequestration of calcium prior to acquiring the F_{min} image. Similar washing and incubation protocols were used to subsequently obtain F_{max} images after 5-minute perfusion with F_{max}-buffer (HBSS, 5μM IM, and 10mM $CaCl_2$). Calcium conversion from fluorescence and the calculations of waveform parameters were performed in MATLAB.

7. Calcium calibration

Stable HeLa-melanopsin cells were grown on collagen-coated coverslips and dye-loaded as described in Section 6: Calcium imaging. Cells were perfused with buffer containing 5μM IM and calcium calibration samples prepared from stock calibration standard (Biotium 59100), and imaged as described above. Fluorescence intensities of individual cells were averaged, and the natural logarithm of normalized fluorescence measurements were plotted against that of calcium concentration. A linear regression was fit to the data in Excel to derive Equation 3 (R-squared of 0.93).

$$\ln\left[\frac{F-F_{min}}{F_{max}-F}\right] = 0.7618 \cdot \ln\left[Ca^{2+}\right] + 0.149 \qquad \textbf{Equation 3}$$

8. Data analyses and calculation of calcium waveform parameters

Data analyses were performed using MATLAB. Fluorescence intensity of an individual cell was converted to absolute calcium concentration using its corresponding F_{min} and F_{max} (Equation 3). The average trace for each illumination paradigm was calculated by averaging the signal from individual cells for each sample. The area under the curve (AUC) was calculated from the baseline-corrected trace over the two minutes following melanopsin stimulation initiation (or the typical fall to baseline). The mean AUC and peaks for each experiment were calculated by averaging the AUC and peaks of all single-cell traces from 6 coverslips (3 epochs per cell, 306-490 cells in total).

9. Transcriptional Activation

Cells were seeded in clear-bottom black 24-well plates (Perkin Elmer 1450-605) at a density of 100,000 cells/well. After 24 hours, cells were transfected with 0.5μg of pGL4.30 plasmid per well using TransIT-LT1 transfection reagent (Mirus Bio 2305) in Opti-MEM (Invitrogen 31985070). At 24-hours post-transfection, the cell media was replaced with phenol-free DMEM containing 2μM all-trans retinal. The plates were placed under custom illuminators (See **Section 11: Illuminator construction and programming**), which were programmed through Arduino microcontroller to deliver light that recapitulated calcium imaging irradiance and pulse sequences to create calcium transients of matching duty ratio or frequency after period adjustment. The cells were irradiated for 6 hours in a humidified incubator at 37°C and 5% CO_2, and subsequently collected for luciferase reporter quantification (Promega E1501, according to manufacturer protocol) after chemically cell lysing with cell culture lysis reagent (Promega E1531). Luminescence measurements were performed in white 96-well plates (Greiner Bio-One T-3025-14), using a Tecan M200 plate reader (5s integration time).

10. Identification of NFAT Ca^{2+} half-saturation binding

HeLa-melanopsin cells were bathed in calibration buffer and assayed for steady-state transcriptional activation level using a luciferase reporter under the regulatory control of the NFAT promoter (see **Section 9: Transcriptional Activation**), in the absence of optical stimulation. The calibration buffer contains HBSS, 0.2% BSA, 1mM MgCl2, 0.5mM EGTA, 5μM IM, and varying concentrations of $CaCl_2$ yielding free calcium concentrations of 0, 0.16, 0.35, 0.54, 0.74, and 1.3 μM. The assay was performed in triplicate for each buffer. Expression was normalized to the minimum and maximum luminescence signals, $[(R-R_{min})/(R_{max}-R_{min})]$ (**Figure S1C**). The data were fit to a Hill equation, with best-fit values of Hill coefficient (n) = 3.01 and calcium half-saturation binding (K_s) = 0.20 μM (R-squared of 0.99).

11. Illuminator construction and hardware programming

The illuminator consists of two layers of acrylic scaffold for a plate positioning and LED alignment, and two custom PCBs designed for independent control of each LED column via Arduino automation of pulse sequences and tuning of irradiance (measured on a ThorLabs PM100D power meter with S120 sensor) using potentiometers (Trimpot, 3362H-102LF). The acrylic layers (**Figure S2A**) were designed in Solid-Works and laser-cut (Universal Laser Systems, Model No. VLS 3.50), to align 5mm dome-cap LEDs to a standard 24-well plate (Joe Knows Electronics, 5-Round-B-100). The PCB boards were designed in Eagle CAD and printed by Custom Circuit Board LLC, with each column possessing four parallel-connected LEDs, a 1kΩ variable potentiometer, and wire terminal for microcontroller-interfacing (**Figure S2B**). All LEDs were quality-controlled prior to assembly for similar output, as measured by an optical power meter. The individual layers were aligned using laser-cut holes assembled with 2-56 machine screws and narrow hex nuts, as shown in main text Figure 2. A zip file containing all Solid-Works CAD files will be permanently available for download at the University of Pennsylvania Scholarly Commons (http://repository.upenn.edu/).

C. Supplemental References (not found in Main Text)

Akerboom, J., Carreras Calderon, N., Tian, L., Wabnig, S., Prigge, M., Tolo, J., Gordus, A., Orger, M.B., Severi, K.E., Macklin, J.J., *et al.* (2013). Genetically encoded calcium indicators for multi-color neural activity imaging and combination with optogenetics. Front Mol Neurosci *6*, 2.

Saito, K., Chang, Y.F., Horikawa, K., Hatsugai, N., Higuchi, Y., Hashida, M., Yoshida, Y., Matsuda, T., Arai, Y., and Nagai, T. (2012). Luminescent proteins for high-speed single-cell and whole-body imaging. Nature communications *3*, 1262.